International Journal of Nanomedicine

Dovepress
open access to scientific and medical research

Open Access Full Text Article

ORIGINAL RESEARCH

Facile synthesis of soybean phospholipid-encapsulated MoS_2 nanosheets for efficient in vitro and in vivo photothermal regression of breast tumor

This article was published in the following Dove Press journal:
International Journal of Nanomedicine
29 April 2016
Number of times this article has been viewed

Xiang Li[1]
Yun Gong[2,3]
Xiaoqian Zhou[1]
Hui Jin[1]
Huanhuan Yan[1]
Shige Wang[2]
Jun Liu[1]

[1]Department of Breast-Thyroid Surgery, Shanghai General Hospital of Nanjing Medical University, Shanghai, People's Republic of China; [2]College of Science, University of Shanghai for Science and Technology, [3]Shanghai Publishing and Printing College, Shanghai, People's Republic of China

Abstract: Two-dimensional MoS_2 nanosheet has been extensively explored as a photothermal agent for tumor regression; however, its surface modification remains a great challenge. Herein, as an alternative to surface polyethylene glycol modification (PEGylation), a facile approach based on "thin-film" strategy has been proposed for the first time to produce soybean phospholipid-encapsulated MoS_2 (SP-MoS_2) nanosheets. By simply vacuum-treating MoS_2 nanosheets/soybean phospholipid/chloroform dispersion in a rotary evaporator, SP-MoS_2 nanosheet was successfully constructed. Owing to the steric hindrance of polymer chains, the surface-coated soybean phospholipid endowed MoS_2 nanosheets with excellent colloidal stability. Without showing detectable in vitro and in vivo hemolysis, coagulation, and cyto-/histotoxicity, the constructed SP-MoS_2 nanosheets showed good photothermal conversion performance and photothermal stability. SP-MoS_2 nanosheet was shown to be a promising platform for in vitro and in vivo breast tumor photothermal therapy. The produced SP-MoS_2 nanosheets featured low cost, simple fabrication, and good in vivo hemo-/histocompatibility and hold promising potential for future clinical tumor therapy.

Keywords: soybean phospholipid, MoS_2 nanosheets, in vivo, photothermal regression, breast tumor

Introduction

Although currently available cancer therapy strategies such as surgery, radiotherapy, and chemotherapy have been extensively applied to clinically treat malignant tumors, cancer is still one of the fatal diseases worldwide.[1,2] The three aforementioned cancer-treating methods always have various shortcomings such as wounds or damage to patients,[3] multidrug resistance,[4,5] or radioresistance.[6,7] To date, it remains a great challenge to develop a novel therapeutic approach with high antitumor efficacy in a minimally invasive manner. Near-infrared (NIR) laser-induced tumor photothermal therapy (PTT) has been deemed as a minimally invasive or noninvasive antitumor approach.[8,9] PTT uses NIR laser, which has a high tissue-penetrating ability, as the energy source, and nanomaterial, which can absorb and convert NIR laser into heat as photothermal agent (PTA), to raise the local temperature of tumor and ablate tumor tissue.[10,11]

MoS_2 nanosheet, a member of the two-dimensional (2D) transition metal dichalcogenide, has found diverse applications in tumor PTT. MoS_2 nanosheets can be either "top–down" exfoliated[12–15] or "bottom–up" synthesized.[16,17] Here, we report a facile

Correspondence: Shige Wang
College of Science, University of Shanghai for Science and Technology, Number 334 Jungong Road, Shanghai 200093, People's Republic of China
Tel +86 21 6571 0384 ext 327
Email sgwang@usst.edu.cn

Jun Liu
Department of Breast-Thyroid Surgery, Shanghai General Hospital of Nanjing Medical University, Number 100 Haining Road, Shanghai 200080, People's Republic of China
Tel +86 21 6324 0090
Email liujun95039@163.com

submit your manuscript | www.dovepress.com
Dovepress
http://dx.doi.org/10.2147/IJN.S104198

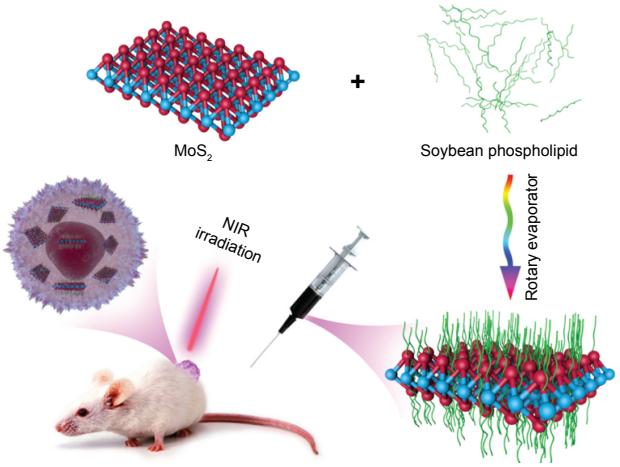

Figure 1 Schematic illustration of the preparation of SP-MoS_2 nanosheets and in vivo PTT.
Abbreviations: PTT, photothermal therapy; NIR, near-infrared; SP-MoS_2, soybean phospholipid-encapsulated MoS_2.

"thin-film" approach to producing soybean phospholipid-encapsulated MoS_2 nanosheets (SP-MoS_2). Soybean phospholipid is a very common polymer, which can be obtained on a large scale. Soybean phospholipid and MoS_2 nanosheet can be readily dissolved or dispersed in chloroform and can form a homogenous dispersion. After vacuum-treating the dispersion in a rotary evaporator, the volatile chloroform will completely evaporate and the soybean phospholipid can be simply coated on the surface of MoS_2 nanosheets (as shown in Figure 1). The excess soybean phospholipid chains that were not encapsulated on the MoS_2 surface can be easily washed using water or saline. Owing to the steric hindrance of polymer chains, the surface-decorated soybean phospholipid chains could confer MoS_2 nanosheets with excellent colloidal stability in physiological environment. The constructed SP-MoS_2 nanosheet showed good photothermal conversion performance and photothermal stability and was employed as PTA for highly efficient in vitro and in vivo PTT against breast tumor. To better illustrate the clinical translational potential, the cyto-, hemo-, and histocompatibility were systematically studied.

Experimental design

Materials

Ammonium tetrathiomolybdate ($[NH_4]_2MoS_4$) was bought from J&K Scientific Co., Ltd. (Shanghai, People's Republic of China). Soybean phospholipid was purchased from Sigma-Aldrich Co. (St Louis, MO, USA). Monoethanolamine was bought form Sinopharm Chemical Reagent Co., Ltd., (Shanghai, People's Republic of China). Mouse fibroblasts (L929) and murine breast cancer (4T1) cells were purchased from the Institute of Biochemistry and Cell Biology (Shanghai, People's Republic of China). Dulbecco's Modified Eagle's Medium (DMEM), Roswell Park Memorial Institute Medium 1640 (RPMI-1640), fetal bovine serum (FBS), penicillin, and streptomycin were purchased from Hangzhou Jinuo Biomedical Technology (Hangzhou, People's Republic of China). Cell counting kit-8 (CCK-8) was purchased from Beyotime Co., Ltd. (Shanghai, People's Republic of China). Trypan blue dye was obtained from Sigma. Balb/c nude mice and Kuming (KM) mice (4–6 weeks old, with the body weight of ~20 g) were purchased from Shanghai Slac Laboratory Animal Center (Shanghai, People's Republic of China). All animal experiments were performed per the guidelines of Shanghai General Hospital of Nanjing Medical University Laboratory Animal Center and the policies of National Ministry of Health and the study was approved by the Ethics Committee of Shanghai General Hospital. All chemicals were directly used as received. Water used in this study was purified with a Pall Cascada laboratory water system (Pall Corporation, New York, NY, USA), with resistivity higher than 18.2 MΩ·cm.

Preparation of MoS_2 and SP-MoS_2 nanosheets

MoS_2 nanosheets were synthesized using a hydrothermal method as previously reported.[16] Briefly, 300 mg $(NH_4)_2MoS_4$ powder was dissolved in 60 mL water to form a $(NH_4)_2MoS_4$ solution. Then, this solution was transferred into a 100 mL polyphenylene-lined stainless steel autoclave and maintained in an oven at 220°C for 12 hours. The raw MoS_2 nanosheets were washed with monoethanolamine solution (50%, in ethanol, v/v) and water several times to get pure MoS_2 nanosheets.

SP-MoS_2 nanosheets were produced by a "thin-film" method (Figure 1). Typically, soybean phospholipid or MoS_2 nanosheet at a concentration of 2.5 or 0.5 mg/mL, respectively, was dissolved or dispersed into chloroform and ultrasonicated for 30 minutes in an ice bath at 4°C to form a homogenous dispersion. The dispersion was then vacuumed at 60°C in a rotary evaporator for 3 hours to evaporate the chloroform. Thereafter, phosphate-buffered saline (PBS) was added to disperse the SP-MoS_2 film under an ultrasonicator (30 minutes, 500 W). The SP-MoS_2 dispersion was stored at room temperature to allow the large aggregates to precipitate, and then it was kept at 4°C for future use. Mo concentration was quantified using an Agilent 700 Series ICP-OES (Agilent Technologies, Santa Clara, CA, USA).

Characterizations

The microstructure of nanosheets of MoS_2 was observed using transmission electron microscopy in a JEOL-2100F

analytical electron microscope (JEOL Ltd., Tokyo, Japan), which was operated at 200 kV. Field-emission scanning electron microscopy (FESEM) was performed with the FEI Magellan 400 field-emission microscope (FEI, Hillsboro, OR, USA). UV-3600 Shimadzu UV-Vis-NIR spectrometer (Shimadzu, Kyoto, Japan) was used to analyze the UV-Vis-NIR spectra of SP-MoS_2 nanosheets. The diameters of pure MoS_2 and SP-MoS_2 nanosheets were measured by dynamic light scattering (DLS) using a Malvern Nano ZS90 Zetasizer Nanoseries system (Malvern Instruments, Malvern, UK) equipped with a standard 633 nm laser.

In vitro cell experiments

DMEM or RPMI-1640 was supplemented with 10% FBS, 100 unit/mL penicillin, and 100 μg/mL streptomycin. L929 or 4T1 cells were cultured in a 10 cm tissue culture dish by adding 10 mL DMEM or RPMI-1640 medium, followed by incubation in a humidified incubator (5% CO_2 at 37°C). For the in vitro cytocompatibility assay, L929 cells (8×10^3 cells per well) were seeded into a 96-well plate and cultured for 24 hours. Then, cells were incubated with pure MoS_2 or SP-MoS_2 at different Mo concentrations (0, 25, 50, and 100 μg/mL). Afterward, the cellular viability was quantified using a CCK-8 kit according to the manufacturer's instruction. Leica DM IL LED inverted phase contrast microscope (Leica Microsystems, Wetzlar, Germany) was used to visualize cellular morphology to qualitatively evaluate the viability of L929 cells. For the in vitro PTT, 8×10^3 4T1 cells in 100 μL RPMI-1640 medium were seeded into an individual well of a 96-well plate and cultured overnight. Then, the medium was replaced with fresh one containing SP-MoS_2 at different concentrations (0, 50, and 100 μg/mL). Cells were then irradiated with an 808 nm laser for 5 minutes, at a power density of 1 W/cm^2. After incubation for another 24 hours, CCK-8 kit and Leica DM IL LED inverted phase contrast microscope were used to quantitatively and qualitatively determine the viability of 4T1 cells. 4T1 cells treated with SP-MoS_2 (100 μg/mL) and NIR were stained with trypan blue to further qualitatively evaluate the cell viability. Cells were washed with PBS three times and incubated with 100 μL trypan blue dye solution (0.4 wt% in PBS) for 3 minutes at 4°C and visualized immediately using Leica DM IL LED inverted phase contrast microscope.

In vitro hemolysis and coagulation assays

In vitro hemolysis assay was performed according to our previous study.[17] Briefly, 0.2 mL human red blood cells (HRBCs) was treated with 0.8 mL SP-MoS_2 dispersions at predetermined concentrations (50, 100, 150, and 200 μg/mL, in saline) in a 1.5 mL Eppendorf tube. HRBCs treated with water or saline were set as positive or negative control, respectively. After incubation at 37°C for 1 hour, the set of suspensions were separated by centrifugation (10,000 rpm, 1 minute). The hemolytic percentage (HP) can be calculated using the following equation:[18]

$$\mathrm{HP}\ (\%) = \frac{D_t - D_{nc}}{D_{pc} - D_{nc}} \times 100\% \quad (1)$$

where D_t, D_{pc}, and D_{nc} represent the absorbance of the supernatant at 541 nm of the test sample, positive and negative controls, respectively. Note that the absorbance of the supernatants at 541 nm is in linear relation to the hemoglobin concentration. For the in vitro blood coagulation assay, blood plasma was treated with SP-MoS_2 dispersions at predetermined concentrations (50, 100, 150, and 200 μg/mL, in saline). The ACL™ 200 blood coagulation analyzer (Instrumentation Laboratory, Bedford, MA, USA) and HemosIL™ (Instrumentation Laboratory) kits were used to determine the typical coagulation parameters including prothrombin time (PT), activated partial thromboplastin time (APTT), and fibrinogen (FIB).

In vitro and in vivo PTT

In vitro photothermal performance of SP-MoS_2 nanosheets was tested and analyzed by irradiating an individual hole of a 96-well cell culture plate containing 100 μL SP-MoS_2 nanosheets dispersion with different Mo concentrations. NIR laser beam was produced using an 808-nm high-power multimode pump laser (Shanghai Connet Fiber Optics Company, Shanghai, People's Republic of China). The temperature and thermal images of the aqueous dispersion at different time points were recorded using the FLIR™ A325SC camera (FLIR Systems, Inc., Wilsonville, OR, USA).

Healthy Balb/c nude mice were subcutaneously injected on the back with 150 μL serum-free RPMI-1640 culture medium containing 1×10^6 4T1 cells. After ~2 weeks, tumor nodules attained a volume of ~0.5 cm^3, and the mice were randomly divided into three groups (n=13 per group). Then, 200 μL saline (group 1), 200 μL SP-MoS_2 dispersion (group 2, [Mo] =200 μg/mL), or 20 μL SP-MoS_2 dispersion (group 3, [Mo] =200 μg/mL) was intravenously (IV, groups 1 and 2) or intratumorally (IT, group 3) injected into each mouse. The tumors were then treated with NIR irradiation (0.8 W/cm^2, 808 nm) for 5 minutes (as shown in Figure 1) immediately (groups 1 and 3) or 12 hours (group 2) postinjection. Then, one mouse in each group was euthanized

and the tumor was fixed immediately for further CD31, Ki67 immunohistochemical staining and terminal deoxynucleotidyl transferase dUTP nick end labeling (TUNEL) assay to compare the therapy efficacy. The long-term therapy outcome was monitored by recording relative tumor volume (V/V_0, where V_0 represents the initiated tumor volume, while V represents the current tumor volume at different time points), tumor appearance, and survival rate (by dividing the number of surviving mice with 12, the number of total mice) of each group.

In vivo biosafety analysis

Hematoxylin–eosin (H&E) staining was performed to analyze the long-term in vivo biosafety of SP-MoS_2 nanosheets. Briefly, KM mice were anesthetized and IV injected with 200 μL saline or SP-MoS_2 dispersion ([Mo] =200 μg/mL, in saline). The body weight of KM mice was recorded every 2 days. After 4 weeks of feeding, KM mice were euthanized, and major organs (heart, liver, spleen, lung, and kidney) were fixed with 10% neutral buffered formalin, embedded in paraffin, and sectioned into slices with a thickness of 8 μm. These slices were finally stained with H&E and photographed using a Leica DM IL LED, inverted phase contrast microscope. For the in vivo hemocompatibility assessment, KM mice were anesthetized, and the heart was punctured to collect blood 14 days after IV injection. Routine blood parameters including white blood cell (WBC) and red blood cells (RBC) count, mean corpuscular hemoglobin (MCH), hematocrit (HCT), mean corpuscular hemoglobin concentration (MCHC), hemoglobin (HGB), mean corpuscular volume (MCV), and red cell distribution width (RDW) were recorded with a Sysmex XS-800i automated hematology analyzer (Sysmex, Kobe, Japan).

For the in vivo biodistribution assay, KM mice were IV injected with 100 μL SP-MoS_2 dispersion ([Mo] =200 μg/mL, in saline). At 6 or 24 hours postadministration, mice were euthanized and major organs (heart, liver, spleen, lung, and kidney) were harvested for distribution analysis. The major organs were digested with aqua regia solution overnight. Mo amounts per unit mass of different organs were quantified using Agilent 700 Series ICP-OES (Agilent Technologies).

Statistical analysis

One-way analysis of variance statistical analysis was used to calculate the significance of the experimental data. A P-value of 0.05 was selected as the significance level. The results are presented as (*) for probability less than 0.05 ($P<0.05$), (**) for $P<0.01$, and (***) for $P<0.001$.

Results

Preparation and characterization of MoS_2 and SP-MoS_2 nanosheets

MoS_2 nanosheets with diameters of ~50 nm could be hydrothermally prepared (Figure S1), based on our previous study methodology.[16] The surface modification of MoS_2 nanosheets with soybean phospholipid did not significantly alter the morphology of nanosheets. The produced SP-MoS_2 nanosheets retained the pristine nanosheet morphology (Figure 2A). SP-MoS_2 nanosheets possess an excellent colloidal stability in water, saline, and RPMI-1640 medium. As shown in Figure S2, the DLS diameter of SP-MoS_2 nanosheets in water, saline, or RPMI-1640 medium had not changed even after 2 days. However, pure MoS_2 nanosheets tend to aggregate in saline even after 1 day (the DLS diameter changed from 150.7 to 122.4 nm, as shown in Figure S3).

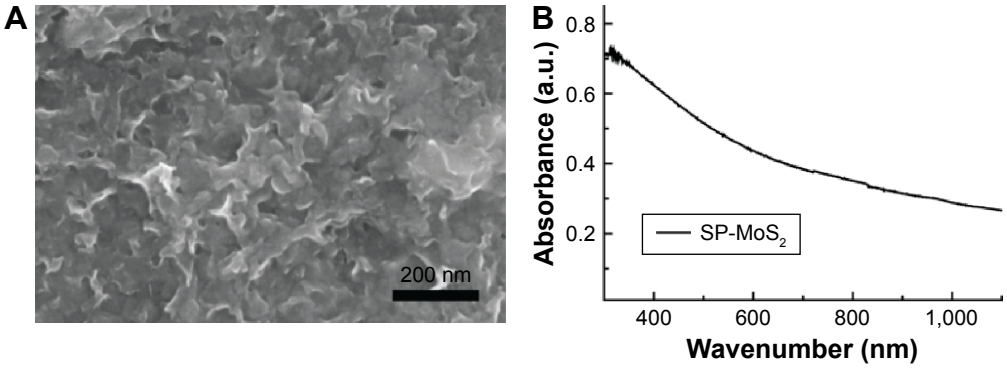

Figure 2 Characterizations of SP-MoS_2 nanosheets.
Notes: (**A**) FESEM image of SP-MoS_2 nanosheets, and (**B**) UV-Vis-NIR spectrum of SP-MoS_2 nanosheets aqueous dispersion ([Mo] =15 ppm).
Abbreviations: FESEM, field-emission scanning electron microscopy; NIR, near-infrared; SP-MoS_2, soybean phospholipid-encapsulated MoS_2; UV-Vis, ultraviolet–visible.

In vitro cyto- and hemocompatibility

The viability of L929 cells treated with SP-MoS_2 or pure MoS_2 nanosheets (Figures 3A and S4) at different concentrations was higher than 80% and showed no significant difference in cells treated with saline (control). Figure 3C shows the cellular morphology of L929 after 24 hours of incubation with SP-MoS_2 nanosheets ([Mo] =100 ppm). No visible cell morphology change was detected when comparing with cells treated with saline (Figure 3B). HRBCs incubated with SP-MoS_2 nanosheets at various experimental concentrations showed hemolysis percentages lower than 5% (Figure 4A, 1.9%±1.0%, 2.1%±0.3%, 2.9%±0.7%, and 3.7%±0.9% at Mo concentration of 50, 100, 150, and 200 ppm, respectively). As negative or positive control, saline or water led to no visible or total hemolysis of HRBCs, respectively. Similar to plasma treated with saline, PT, APTT, and FIB values of blood plasma incubated with different concentrations of SP-MoS_2 nanosheets were in the normal range (Figure 4B).

In vitro and in vivo PTT

As shown in Figure 5A and B, SP-MoS_2 nanosheets dispersion at a Mo concentration of 100 ppm showed the highest temperature increase at a power density of 1.0 W/cm^2. The highest temperature increase of 14.4°C was achieved after 300 seconds of irradiation. Comparatively, saline showed a negligible photothermal effect even when irradiated for less than 300 seconds at a power density of 1.0 W/cm^2. The corresponding photothermal images (Figure 5B) indicated a consistent photothermal transformation outcome. Meanwhile, SP-MoS_2 nanosheets showed no obvious difference in temperature increment within five cycles of NIR irradiation (Figure S5).

After irradiating the cell culture medium containing different concentrations of SP-MoS_2 nanosheets, the attached 4T1 cells showed a concentration-dependent cell death (Figure 6A, blue bars). However, viability of cells treated with SP-MoS_2 nanosheets but without NIR, or saline with NIR, was not influenced (with cell viability higher than 80%, Figure 6A, red bars). Trypan blue staining (Figure 6B and C) showed that cells treated with saline and NIR laser were alive, while those treated with an SP-MoS_2–containing medium ([Mo] =100 ppm) and NIR laser were killed. NIR irradiation can induce an apparent temperature increase in tumors with IV-injected SP- MoS_2 nanosheets (Figure 7A and B [b_1–b_4], 5.4°C versus 2.4°C of control group, Figure S6), and the temperature increase was more evident in tumors with IT-administered SP-MoS_2 nanosheets (Figure 7C and D [d_1–d_4], a temperature increase of 12.4°C and 16.2°C after 100 and 300 seconds of irradiation, respectively). Immunohistochemical staining showed that tumor with IT or IV materials injection and NIR irradiation exhibited a less expression of CD31 expression than control tumor, and mouse with IT materials injection experienced a less CD31 expression than IV administration (Figure 8). In comparison to tumor treated with saline, IT- or IV-SP-MoS2 administrated mice after NIR irradiation showed an obvious decreased antigen Ki67 expression. Similarly, IT-administered mice after NIR irradiation expressed the lowest antigen Ki67 level.

Since the cell viability was lower than 20% when Mo concentration was 100 ppm, we used a Mo concentration of 100 ppm for the following studies. The tumor volume and appearance of 4T1 tumor-bearing mice after different treatments were recorded (Figure 9). Mice treated with saline showed an uncontrolled tumor growth rate, with tumor size increasing to ~three times the original within the initial 15 days. After 15 days, tumor volume of IV-injected mice was ~1.4 times larger than initial tumor (Figure 9A–C [c_3 and c_4]), while tumor volume of IT-injected mice was halved (Figure 9A–C [c_5 and c_6]). We then monitored the long-term survival rate of mice under different treatments (Figure S7). Mice in the control group died of natural cause, while the life span of SP-MoS_2 nanosheets–treated mice increased.

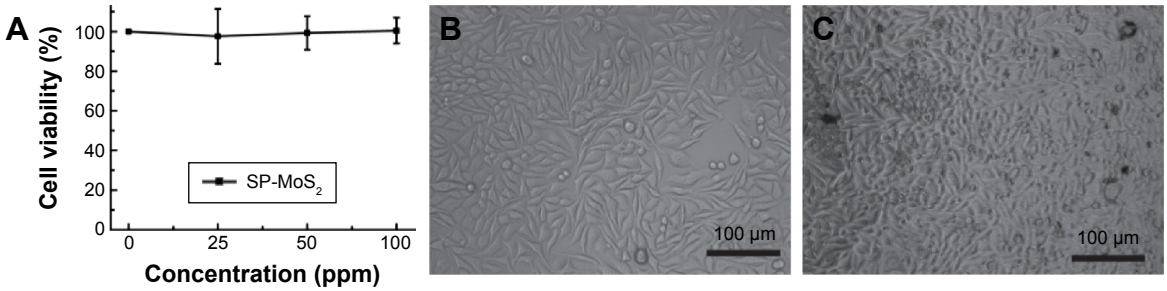

Figure 3 In vitro cell viability.
Notes: (**A**) Cell viability assay of L929 cells after treatment with SP-MoS_2 nanosheets at a given Mo concentrations for 24 hours (mean ± SD, n=3). (**B** and **C**) Phase contrast photos of L929 cells treated with (**B**) saline and (**C**) SP-MoS_2 nanosheets ([Mo] =100 ppm).
Abbreviations: SD, standard deviation; SP-MoS_2, soybean phospholipid-encapsulated MoS_2.

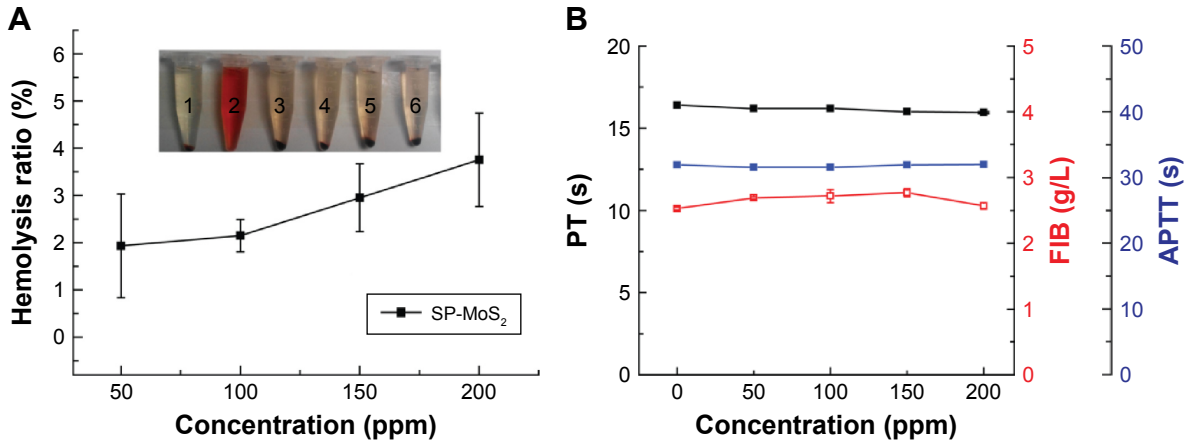

Figure 4 In vitro hemolysis and coagulation assays.
Notes: (**A**) Hemolysis ratio of HRBCs after 1 hour incubation with SP-MoS_2 at different concentrations. The photograph shows the centrifuged HRBCs suspensions after treating with 1) saline, 2) water, and 3) SP-MoS_2 nanosheets with different Mo concentrations (3:50 ppm, 4:100 ppm, 5:150 ppm, and 6:200 ppm) for 1 hour. (**B**) PT, FIB, and APTT of blood plasma after treated with SP-MoS_2 nanosheets at noted concentrations.
Abbreviations: APTT, activated partial thromboplastin time; FIB, fibrinogen; HRBCs, human red blood cells; PT, prothrombin time; SP-MoS_2, soybean phospholipid-encapsulated MoS_2.

In vivo biosafety evaluation

As illustrated in Figure 10A and B, routine blood parameters, including WBC, RBC, MCH, HCT, MCHC, HGB, MCV, and RDW, in SP-MoS_2-treated KM mice were in the normal range and showed no significant difference with control (mice treated with saline). There was no distinct weight variation over feeding time in both control and SP-MoS_2-treated KM mice (Figure 10C). No apparent pathological tissue damage or abnormality of major organs in SP-MoS_2 nanosheets–treated KM mice can be detected from H&E staining results. The Mo amounts in major organs including the heart, liver, spleen, lung, and kidney was analyzed 6 or 24 hours after injection (Figure S8). Similar to other reported "bottom–up" synthesized[16] or "top–down" exfoliated[14] MoS_2 nanosheets, a majority of the injected Mo was accumulated in the liver and spleen, and the Mo level increased with time during the first 24 hours. Mo amounts in lung and kidney was relatively small, especially in kidney, and the amounts decreased with time in the initial 24 hours.

Discussion

Various PTAs including metal-based PTAs such as Pd nanosheets,[19] carbon-based PTAs such as carbon nanotubes and[20] graphene,[21] conductive polymers such as organic indocyanine green[22] and polypyrrole,[23] and copper chalcogenide nanoparticles such as CuS[24,25] and $Cu_{2-x}Se$,[26] have been

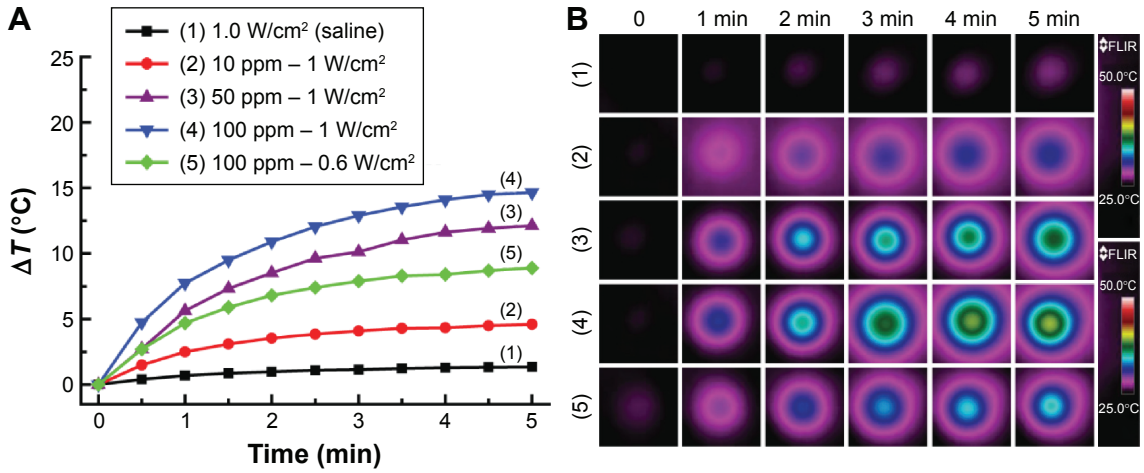

Figure 5 In vitro photothermal conversion of SP-MoS_2 nanosheets.
Notes: (**A**) Power density/concentration-dependent temperature change curves and (**B**) the corresponding thermal images under continuous irradiation with an 808 nm laser. ΔT represents the temperature increment.
Abbreviations: SP-MoS_2, soybean phospholipid-encapsulated MoS_2; min, minutes.

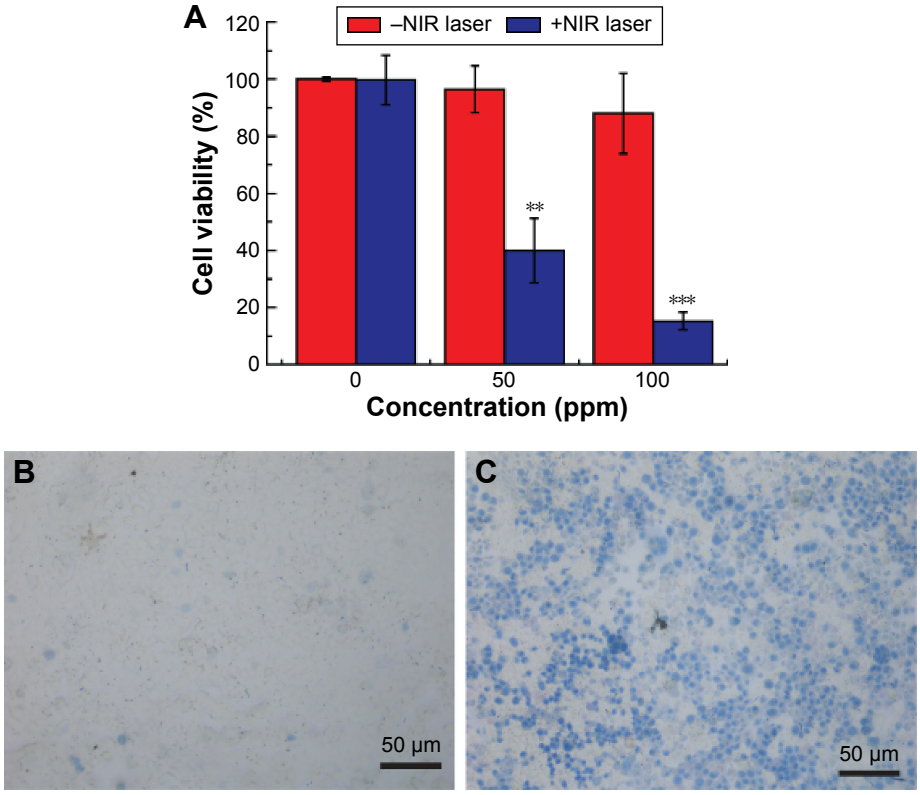

Figure 6 In vitro PTT.

Notes: (**A**) 4T1 cell viability treated with or without 808 nm NIR laser (5 minutes, 1 W/cm^2), cells were coincubated with SP-MoS_2 nanosheets with different Mo concentrations as shown in *x*-axis (mean ± SD, n=3). (**B** and **C**) Trypan blue staining of 4T1 cells coincubated with SP-MoS_2 without (**B**) and with (**C**) NIR irradiating (5 minutes, 1 W/cm^2). "–" and "+" mean without, with, respectively. The *P* value of 0.05 was selected as the significance level. Data presented as mean ± SD, n = 3, (**) $P<0.01$, and (***) $P<0.001$, respectively.

Abbreviations: NIR, near-infrared; PTT, photothermal therapy; SD, standard deviation; SP-MoS_2, soybean phospholipid-encapsulated MoS_2.

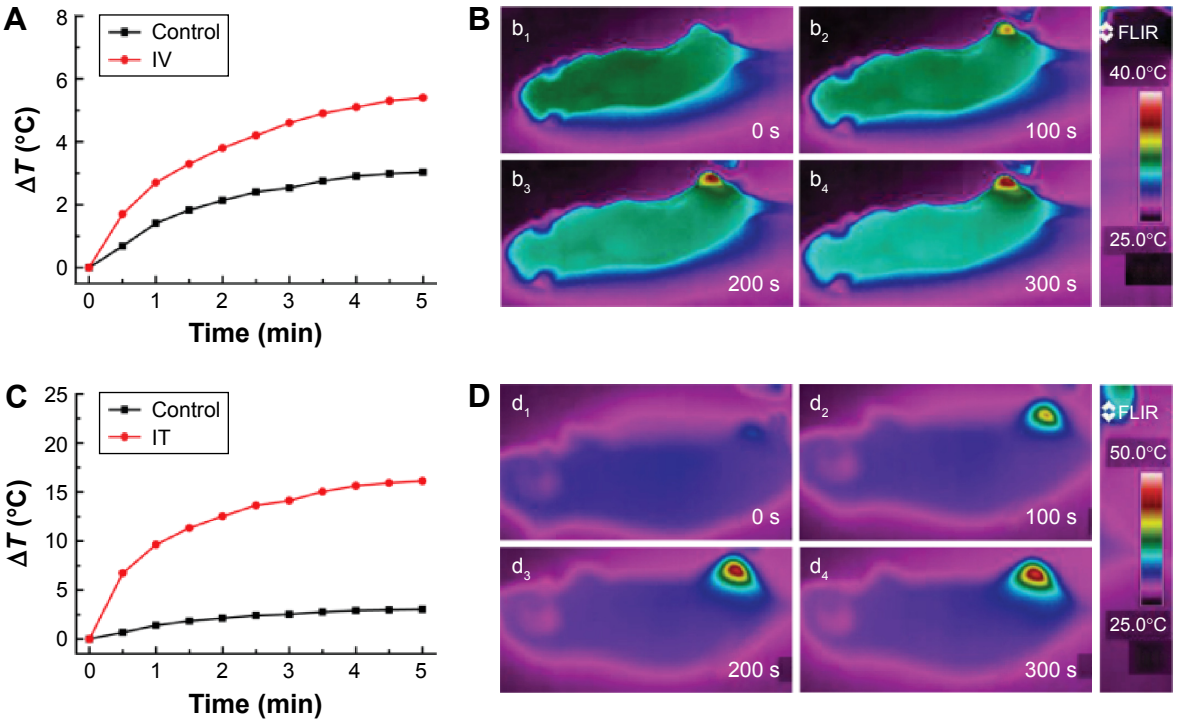

Figure 7 In vivo PTT.

Notes: (**A** and **C**) Temperature change curves of tumor after (**A**) IV or (**C**) IT injection with SP-MoS_2 nanosheets and NIR laser irradiation (5 minutes, 0.8 W/cm^2). (**B**, b_1–b_4) and (**D**, d_1–d_4) Corresponding in vivo thermal images of mouse from panel **A** or **C** after different durations NIR irradiating, respectively.

Abbreviations: IV, intravenous; IT, intratumoral; PTT, photothermal therapy; NIR, near-infrared; SP-MoS_2, soybean phospholipid-encapsulated MoS_2; min, minutes; T, temperature.

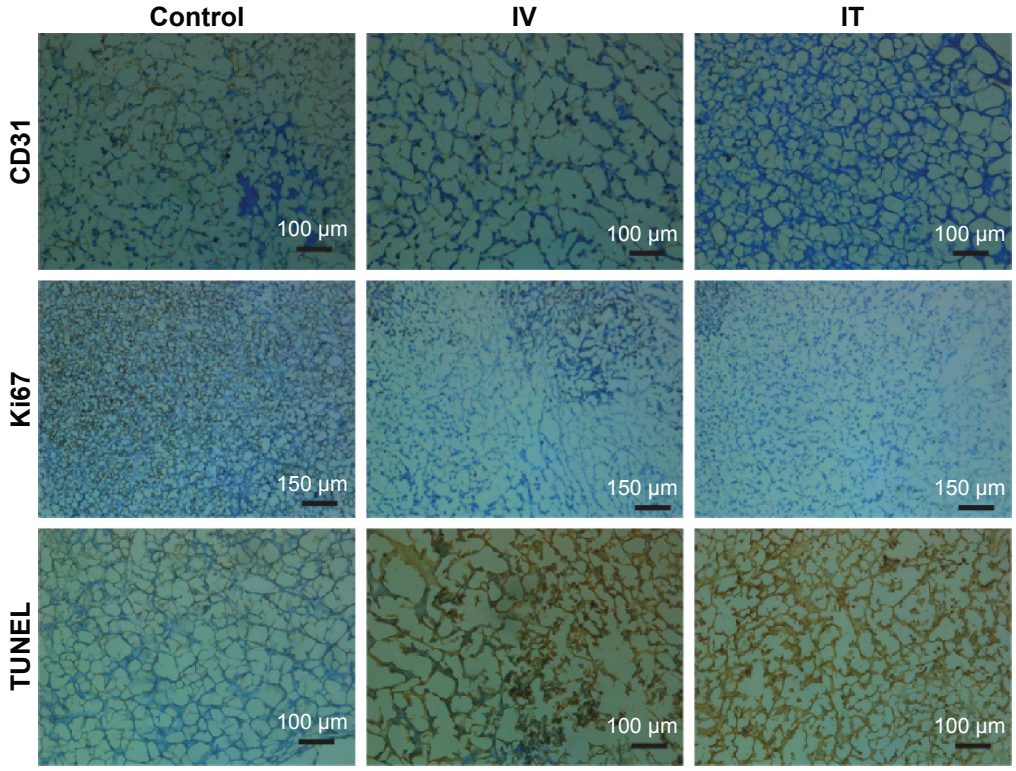

Figure 8 Immunohistochemical staining for CD31, Ki67, and TUNEL analysis of mouse after treatment with saline (control) or SP-MoS_2 nanosheets (IV or IT injection).
Abbreviations: IV, intravenous; IT, intratumoral; SP-MoS_2, soybean phospholipid-encapsulated MoS_2; TUNEL, terminal deoxynucleotidyl transferase dUTP nick end labeling.

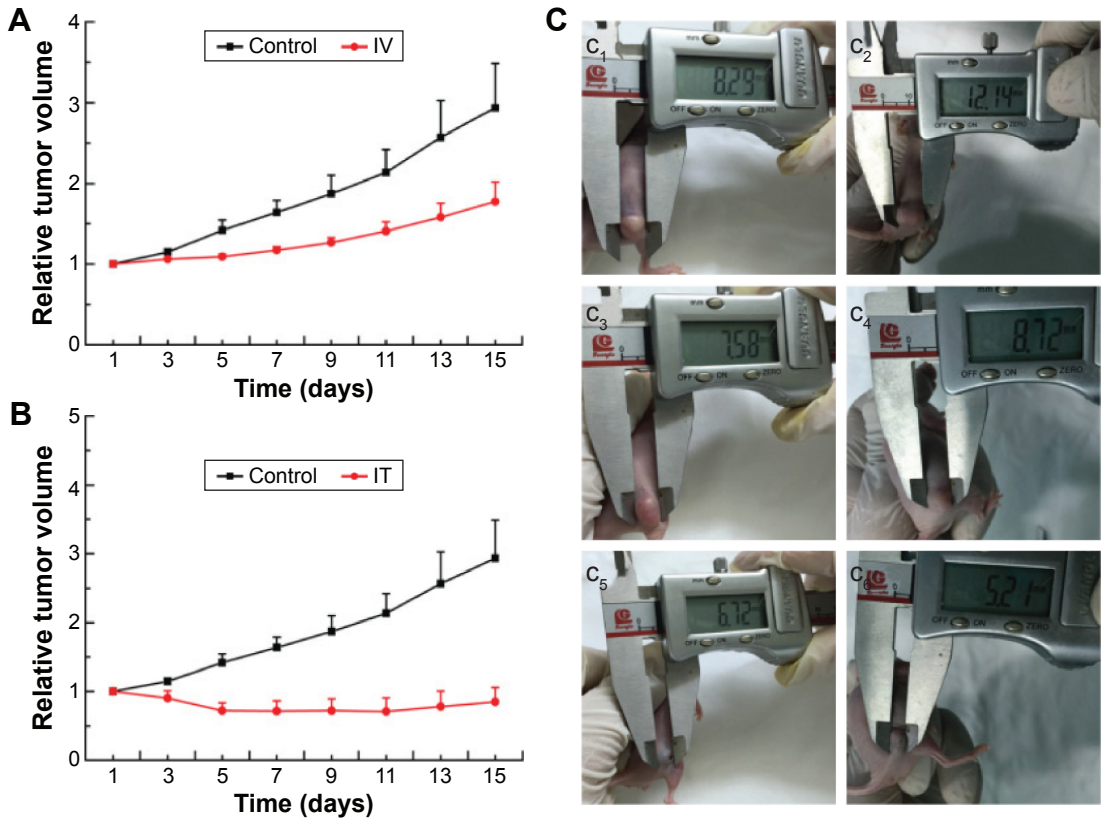

Figure 9 The tumor volume and appearance.
Notes: (**A** and **B**) Tumor volume of 4T1 mice after different treatments as described. (**C**, c_1–c_6) Digital photos of tumor-bearing nude mice before (c_1, c_3, and c_5) and 15 days after (c_2, c_4, and c_6) PTT (c_1, c_2: control; c_3, c_4: IV administration; c_5, c_6: IT administration), mean ± SD, n=6.
Abbreviations: IV, intravenous; IT, intratumoral; PTT, photothermal therapy; SD, standard deviation; SP-MoS_2, soybean phospholipid-encapsulated MoS_2.

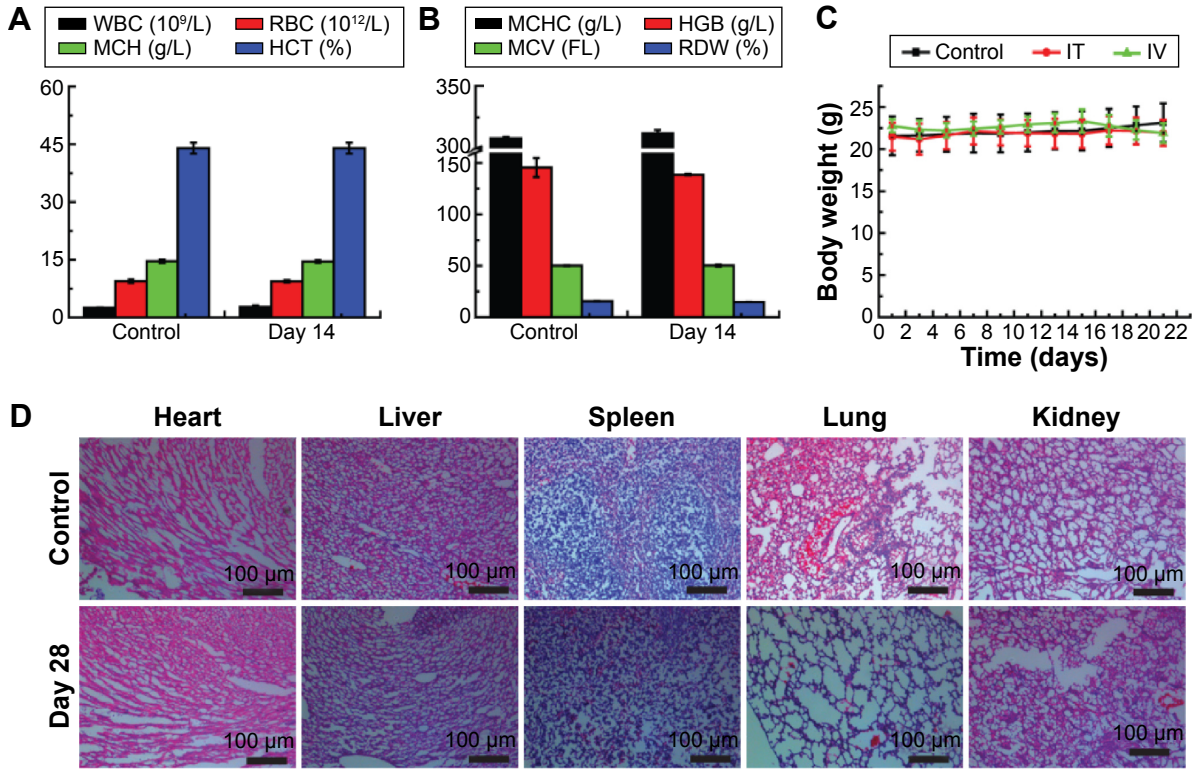

Figure 10 In vivo compatibility.

Notes: (**A** and **B**) Blood hematology data of KM mice IV injected with saline (control) or 14 days after injection with SP-MoS_2 nanosheets ([Mo] =200 μg/mL). (**C**) Body weight of KM mice after different treatments (mean ± SD, n=3). (**D**) H&E staining of major organs (heart, liver, spleen, lung, and kidney) from mouse treated with saline (control) or SP-MoS_2 nanosheets ([Mo] =200 ppm, magnification: 100×).

Abbreviations: HGB, hemoglobin; HCT, hematocrit; H&E, hematoxylin–eosin; IV, intravenous; KM, Kuming; MCH, mean corpuscular hemoglobin; MCHC, mean corpuscular hemoglobin concentrations; MCV, mean corpuscular volume; RBC, red blood cell; RDW, red cell distribution width; SD, standard deviation; SP-MoS_2, soybean phospholipid-encapsulated MoS_2; WBC, white blood cell.

successfully synthesized. It has been demonstrated that the surface modification of nanomaterials can significantly influence their colloidal stability and biological behavior such as blood circulation durations, biodistribution, and excretion.[17,27] Therefore, it is of vital importance to modify nanomaterials with other polymers to obtain an organic/inorganic composite/hybrid nanomaterial. Liu et al reported on the modification of chemical-exfoliated MoS_2 nanosheets with lipoic acid-modified PEG (LA-PEG) using a thiol reaction.[14] They showed that the surface-anchored LA-PEG could increase the physiological stability and biocompatibility of MoS_2 nanosheets. In another study, Yin et al reported on the decoration of intercalation-exfoliated MoS_2 nanosheets with chitosan (CS) for combined tumor chemotherapy and PTT.[15] In general, the aforementioned methods are based on the inefficient chemical bonding procedures. In a previous study, we reported a "bottom–up" one-pot approach to synchronously completing the synthesis and surface PEGylation of MoS_2 nanosheets or MoS_2/Bi_2S_3 nanosheets.[16,28] Nevertheless, this one-pot modification process tends to change the structure (including diameter, thickness, etc) of the pristine MoS_2 nanosheets. In addition, this method is not suitable for the surface bonding of polymers with active groups, which are sensitive to the high temperature of the hydrothermal duration. On this basis, developing an alternative facile method that can simply produce 2D MoS_2 nanosheets with excellent colloidal stability and therapeutic performance is of high importance for the biomedical applications of 2D MoS_2 nanosheets.

Soybean phospholipid is a kind of natural phospholipid that is widely distributed in plants; therefore, the cost of isolating soybean from natural sources is always lower than that of synthesizing or semisynthesizing.[17] More interestingly, soybean phospholipid possesses an excellent biocompatibility and amphiphilicity and can form a stable biomembrane on the surface of nanomaterials.[29] Based on these merits, we explored a facile "thin-film" approach to encapsulating soybean phospholipid on the surface of MoS_2 nanosheets. The ultrasonic treatment of SP-MoS_2/soybean phospholipid/chloroform dispersion will allow the complete contact of SP-MoS_2 nanosheets with soybean phospholipid chains. With the rapid volatility of chloroform, the soybean phospholipid chains could automatically be encapsulated and form a multilayer thin-film

on MoS_2 surface and render SP-MoS_2 excellent colloidal stability owing to the steric hindrance of its polymer chains (Figure 1).

DLS results confirmed that SP-MoS_2 nanosheets possessed an excellent colloidal stability in different environments (Figure S2), which will greatly favor the applications of SP-MoS_2 nanosheets. A promising nanoplatform for tumor PTT should be cyto-, hemo-, and histocompatible; therefore, we studied the cyto-, hemo-, and histocompatibility of the constructed SP-MoS_2 nanosheets before the analysis of in vivo PTT performance. Quantitative and qualitative cytocompatibility evaluations using CCK-8 assay and cell morphology observation demonstrated the excellent cytocompatibility of SP-MoS_2 nanosheets (Figure 3). The hemocompatibility was proven via in vitro hemolysis and coagulation assays. The hemolysis percentages of HRBCs incubated with different concentrated SP-MoS_2 nanosheets were lower than 5% (Figure 4A), indicating that SP-MoS_2 nanosheets possess a good hemocompatibility in experimental concentrations.[30] The in vitro coagulation assay (Figure 4B) proved that SP-MoS_2 nanosheets would not influence the coagulation function of blood. Inspired by this excellent in vitro cyto- and hemocompatibility, we then studied the in vitro and in vivo PTT outcome on a breast tumor-bearing nude mice model. SP-MoS_2 nanosheets can absorb greater NIR laser beams at a wavelength of 808 nm than at 980 nm (Figure 2B). Therefore, as a representative, we selected NIR laser with a wavelength of 808 nm as the power source for in vitro and in vivo PTT study. Similar to the "bottom–up" synthesized[16] or "top–down" exfoliated[12–14] MoS_2 nanosheets, SP-MoS_2 nanosheets can not only efficiently absorb NIR laser (wavelength: 700–1100 nm, Figure 2B) but also transform the absorbed laser into heat. The photothermal behavior of SP-MoS_2 nanosheets is closely related to the Mo concentration and laser power density (Figure 5A and B), ie, the temperature increment (ΔT) increased with Mo concentration and power density. Importantly, SP-MoS_2 nanosheets showed high photothermal stability (Figure S5). SP-MoS_2 could significantly kill cancer cells via transforming the absorbed NIR light into heat, and in vitro PTT assay showed that SP-MoS_2 nanosheets could efficiently enhance the temperature to the critical temperature (42°C)[31] for tumor PTT, enabling efficient cell death and tumor coagulation necrosis. It is worth noting that IV- or IT-injected SP-MoS_2 nanosheets were accumulated at tumor site because of the passive enhanced permeability retention (EPR) effect. That is, a portion of the IV-injected SP-MoS_2 nanosheets can accumulate at tumor site because of the EPR effect of tumor vessel, causing a temperature increase under NIR irradiation (Figure 7A and B [b_1–b_4], 5.4°C versus 2.4°C of control group, Figure S6). While much more of the IT-injected SP-MoS_2 nanosheets could remain in tumor site, thus showing a faster tumor temperature elevation (Figure 7C and D [d_1–d_4], a temperature increase of 12.4°C and 16.2°C after 100 and 300 seconds of irradiation, respectively). The in vivo tumor PTT performance was compared using the immunohistochemical staining approach, including CD31, Ki67, and TUNEL analysis after the PTT (Figure 8). In immunohistochemical staining, a lower CD31 expression represents a less CD31-positive tumor microvessel angiogenesis and a stronger inhibition of cancer cells, and more expression of antigen Ki67 indicates a higher tumor cell proliferation.[32] As expected, results of CD31, Ki67, and TUNEL assay clearly indicate that the SP-MoS_2 nanosheets could effectively kill tumor cells and significantly inhibit tumor growth: the IT-administered SP-MoS_2 nanosheets were the best at killing tumor cells, followed by the IV- injected one, with saline coming in last. The tumor volume and appearance of 4T1 tumor-bearing mice after different treatments were recorded (Figure 9). Tumor growth of SP-MoS_2-treated mice (regardless of the IT or IV injection) after NIR irradiation was significantly suppressed. Because of the excellent PTT outcome, the life span of SP-MoS_2 nanosheets–treated mice increased.

Note that tumor growth in IV-injected mice was not totally inhibited, which could be attributed to the low NIR power density (0.8 W/cm^2) and inefficient accumulation of SP-MoS_2 nanosheets at the tumor site. Nanomaterials with certain surface-targeting ligand(s) will enable a higher tumor uptake amount;[33,34] therefore, MoS_2 nanosheets with surface-targeting ligand(s) that can efficiently target tumors is the future research emphasis. The in vivo tumor PTT proved that SP-MoS_2 nanosheet was able to serve as a promising platform for efficient breast tumor PTT. Further in vivo hemo- and histocompatibility assays proved that SP-MoS_2 nanosheets could not affect the normal function of blood and metabolism of major organs (Figure 10), even though a large part of the injected SP-MoS_2 nanosheets will be captured by the liver and spleen (Figure S8), similar to many other kinds of nanomaterials.[13,14,16,17] With high in vivo hemo- and histocompatibility and anticancer efficacy, low cost, and simple fabrication, SP-MoS_2 nanosheets hold promising potential for efficient localized tumor therapy.

Conclusion

In summary, a facile "thin-film" strategy has been successfully demonstrated to produce soybean phospholipid-encapsulated

MoS_2 nanosheets. Owing to the steric hindrance of polymer chains, surface-anchored soybean phospholipid could render MoS_2 nanosheets with excellent colloidal stability. The constructed SP-MoS_2 nanosheets showed good in vitro and in vivo cyto-, hemo-, and histocompatibility within experimental concentration ranges. Because of the NIR absorption attribute, SP-MoS_2 nanosheets exhibited good photothermal conversion performance and photothermal stability under NIR irradiation. Importantly, SP-MoS_2 nanosheets showed an excellent in vitro and in vivo anticancer efficacy. Breast tumor growth in mice with IT or IV SP-MoS_2 injection was significantly suppressed. Compared with other reported MoS_2 surface modification methods, the "thin-film" strategy is easy to operate, and the used soybean phospholipid is less expensive and biocompatible. Therefore, the findings in this report will greatly highlight the clinical translational potential of MoS_2 nanosheet in the antitumor therapy field.

Acknowledgments

This work was sponsored by "Chenguang Program" supported by Shanghai Education Development Foundation and Shanghai Municipal Education Commission (14CGB15 for YG, and 15CG52 for SW).The authors also thank the State Key Laboratory of Molecular Engineering of Polymers (K2016-20, Fudan University) for their support.

Disclosure

The authors report no conflicts of interest in this work.

References

1. Jemal A, Bray F, Center MM, Ferlay J, Ward E, Forman D. Global cancer statistics. *CA Cancer J Clin*. 2011;61(2):69–90.
2. Siegel R, Naishadham D, Jemal A. Cancer statistics, 2013. *CA Cancer J Clin*. 2013;63(1):11–30.
3. Xiao Q, Zheng X, Bu W, et al. A core/satellite multifunctional nanotheranostic for in vivo imaging and tumor eradication by radiation/photothermal synergistic therapy. *J Am Chem Soc*. 2013;135(35):13041–13048.
4. Gao Y, Chen Y, Ji X, et al. Controlled intracellular release of doxorubicin in multidrug-resistant cancer cells by tuning the shell-pore sizes of mesoporous silica nanoparticles. *ACS Nano*. 2011;5(12):9788–9798.
5. Li L, Tang F, Liu H, et al. In vivo delivery of silica nanorattle encapsulated docetaxel for liver cancer therapy with low toxicity and high efficacy. *ACS Nano*. 2010;4(11):6874–6882.
6. Hainfeld JF, Dilmanian FA, Slatkin DN, Smilowitz HM. Radiotherapy enhancement with gold nanoparticles. *J Pharm Pharmacol*. 2008;60(8):977–985.
7. Nakae T, Uto Y, Tanaka M, et al. Design, synthesis, and radiosensitizing activities of sugar-hybrid hypoxic cell radiosensitizers. *Bioorg Med Chem*. 2008;16(2):675–682.
8. Shi S, Huang Y, Chen X, Weng J, Zheng N. Optimization of surface coating on small Pd nanosheets for in vivo near-infrared photothermal therapy of tumor. *ACS Appl Mater Interfaces*. 2015;7(26):14369–14375.
9. Zeng L, Pan Y, Wang S, et al. Raman reporter-coupled Ag-core@Au-shell nanostars for in vivo improved surface enhanced raman scattering imaging and near-infrared-triggered photothermal therapy in breast cancers. *ACS Appl Mater Interfaces*. 2015;7(30):16781–16791.
10. Yu M, Guo F, Wang J, Tan F, Li N. Photosensitizer-loaded pH-responsive hollow gold nanospheres for single light-induced photothermal/photodynamic therapy. *ACS Appl Mater Interfaces*. 2015;7(32):17592–17597.
11. Zhao Y, Song W, Wang D, et al. Phase-shifted PFH@PLGA/Fe_3O_4 nanocapsules for MRI/US imaging and photothermal therapy with near-infrared irradiation. *ACS Appl Mater Interfaces*. 2015;7(26):14231–14242.
12. Chou SS, Kaehr B, Kim J, et al. Chemically exfoliated MoS_2 as near-infrared photothermal agents. *Angew Chem Int Ed Engl*. 2013;125(15):4254–4258.
13. Liu T, Wang C, Cui W, et al. Combined photothermal and photodynamic therapy delivered by PEGylated MoS_2 nanosheets. *Nanoscale*. 2014;6(19):11219–11225.
14. Liu T, Wang C, Gu X, et al. Drug delivery with PEGylated MoS_2 nano-sheets for combined photothermal and chemotherapy of cancer. *Adv Mater*. 2014;26(21):3433–3440.
15. Yin W, Yan L, Yu J, et al. High-throughput synthesis of single-layer MoS_2 nanosheets as a near-infrared photothermal-triggered drug delivery for effective cancer therapy. *ACS Nano*. 2014;8(7):6922–6933.
16. Wang S, Li K, Chen Y, et al. Biocompatible PEGylated MoS_2 nanosheets: controllable bottom-up synthesis and highly efficient photothermal regression of tumor. *Biomaterials*. 2015;39:206–217.
17. Wang S, Li X, Chen Y, et al. A facile one-pot synthesis of a two-dimensional MoS_2/Bi_2S_3 composite theranostic nanosystem for multi-modality tumor imaging and therapy. *Adv Mater*. 2015;27(17):2775–2782.
18. Meng ZX, Zheng W, Li L, Zheng YF. Fabrication and characterization of three-dimensional nanofiber membrane of PCL-MWCNTs by electrospinning. *Mater Sci Eng C Mater Biol Appl*. 2010;30(7):1014–1021.
19. Fang W, Tang S, Liu P, Fang X, Gong J, Zheng N. Pd nanosheet-covered hollow mesoporous silica nanoparticles as a platform for the chemothotothermal treatment of cancer cells. *Small*. 2012;8(24):3816–3822.
20. Liu X, Tao H, Yang K, Zhang S, Lee S-T, Liu Z. Optimization of surface chemistry on single-walled carbon nanotubes for in vivo photothermal ablation of tumors. *Biomaterials*. 2011;32(1):144–151.
21. Sheng Z, Song L, Zheng J, et al. Protein-assisted fabrication of nano-reduced graphene oxide for combined in vivo photoacoustic imaging and photothermal therapy. *Biomaterials*. 2013;34(21):5236–5243.
22. Zheng M, Yue C, Ma Y, et al. Single-step assembly of DOX/ICG loaded lipid-polymer nanoparticles for highly effective chemo-photothermal combination therapy. *ACS Nano*. 2013;7(3):2056–2067.
23. Zha Z, Yue X, Ren Q, Dai Z. Uniform polypyrrole nanoparticles with high photothermal conversion efficiency for photothermal ablation of cancer cells. *Adv Mater*. 2013;25(5):777–782.
24. Li Y, Lu W, Huang Q, Li C, Chen W. Copper sulfide nanoparticles for photothermal ablation of tumor cells. *Nanomedicine*. 2010;5(8):1161–1171.
25. Tian Q, Tang M, Sun Y, et al. Hydrophilic flower-like CuS Superstructures as an efficient 980 nm laser-driven photothermal agent for ablation of cancer cells. *Adv Mater*. 2011;23(31):3542–3547.
26. Hessel CM, P. Pattani V, Rasch M, et al. Copper selenide nanocrystals for photothermal therapy. *Nano Lett*. 2011;11(6):2560–2566.
27. Mou J, Li P, Liu C, et al. Ultrasmall $Cu_{2-x}S$ nanodots for highly efficient photoacoustic imaging-guided photothermal therapy. *Small*. 2015;11(19):2275–2283.
28. Chen Q, Wang H, Liu H, et al. Multifunctional dendrimer-entrapped gold nanoparticles modified with RGD peptide for targeted computed tomography/magnetic resonance dug-modal imaging of tumors. *Anal Chem*. 2015;87(7):3949–3956.
29. Kostarelos K, Luckham P, Tadros TF. Addition of block copolymers to liposomes prepared using soybean lecithin. Effects on formation, stability and the specific localization of the incorporated surfactants investigated. *J Liposome Res*. 1995;5(1):117–130.

30. Liu B, Zheng YF. Effects of alloying elements (Mn, Co, Al, W, Sn, B, C and S) on biodegradability and in vitro biocompatibility of pure iron. *Acta Biomater*. 2011;7(3):1407–1420.
31. Shinkai M, Yanase M, Honda H, Wakabayashi T, Yoshida J, Kobayashi T. Intracellular hyperthermia for cancer using magnetite cationic liposomes: in vitro study. *Jpn J Cancer Res*. 1996;87(11):1179–1183.
32. Wang Y, Liu P, Duan Y, et al. Specific cell targeting with aprpg conjugated PEG-PLGA nanoparticles for treating ovarian cancer. *Biomaterials*. 2014;35(3):983–992.
33. Li J, Zheng L, Cai H, et al. Polyethyleneimine-mediated synthesis of folic acid-targeted iron oxide nanoparticles for in vivo tumor MR imaging. *Biomaterials*. 2013;34(33):8382–8392.
34. Li J, He Y, Sun W, et al. Hyaluronic acid-modified hydrothermally synthesized iron oxide nanoparticles for targeted tumor MR imaging. *Biomaterials*. 2014;35(11):3666–3677.

Supplementary materials

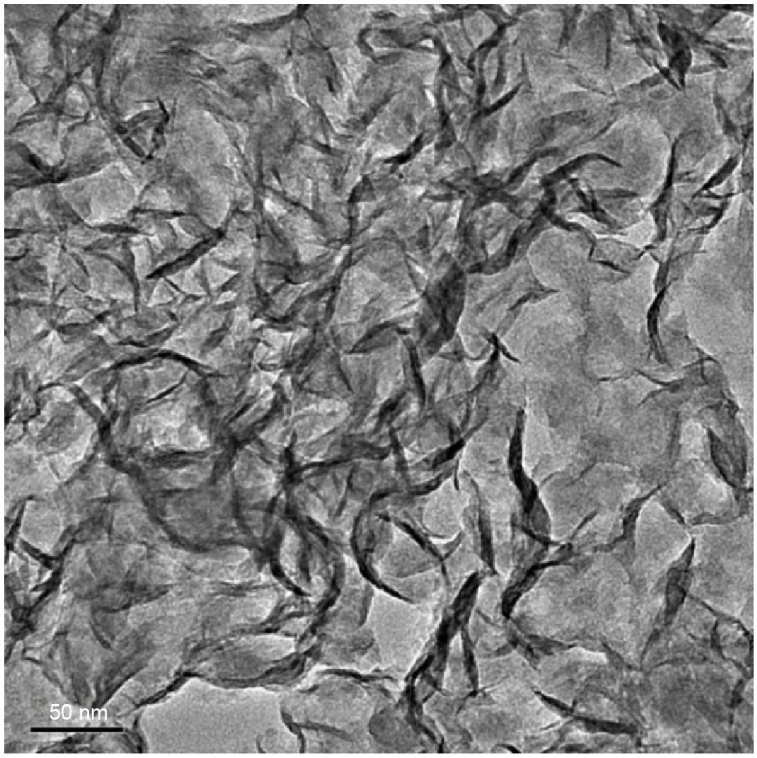

Figure S1 TEM image of MoS_2 nanosheets.
Abbreviation: TEM, transmission electron microscope.

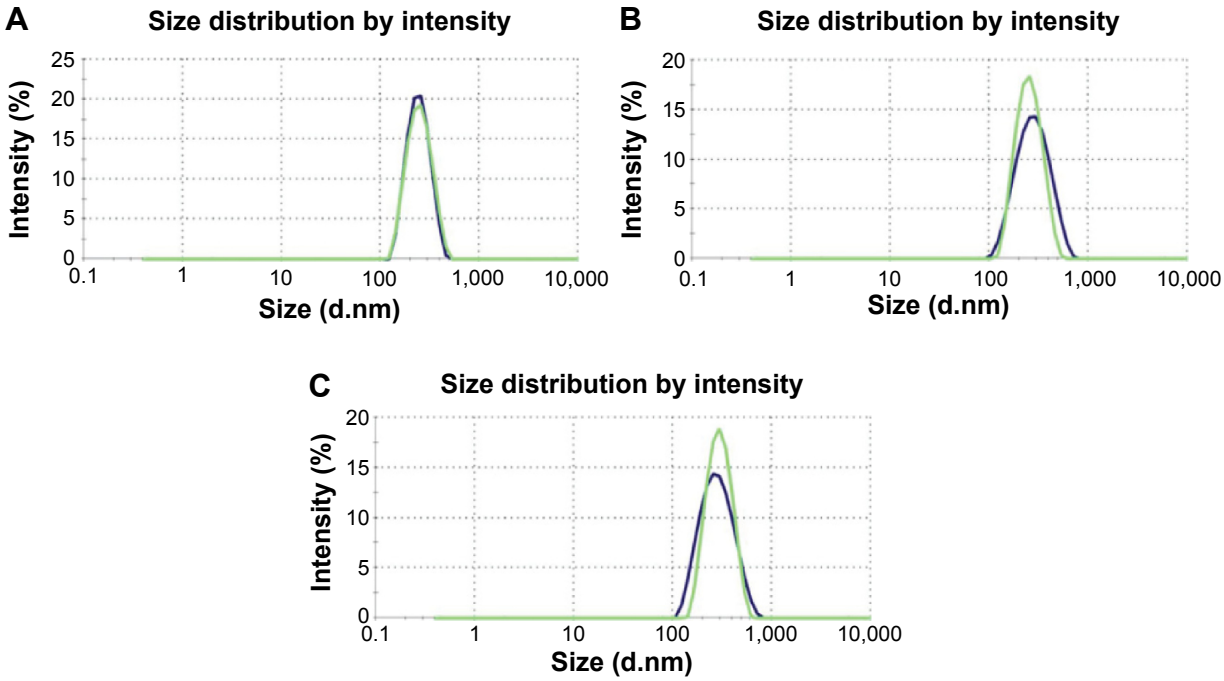

Figure S2 DLS diameters of SP-Mos2 nanosheets.
Notes: DLS diameters of SP-MoS_2 nanosheets in (**A**) water, (**B**) saline, and (**C**) RPMI-1640 medium before (blue) and after (green) 2 days.
Abbreviations: DLS, dynamic light scattering; SP-MoS_2, soybean phospholipid-encapsulated MoS_2; RPMI-1640, Roswell Park Memorial Institute-1640.

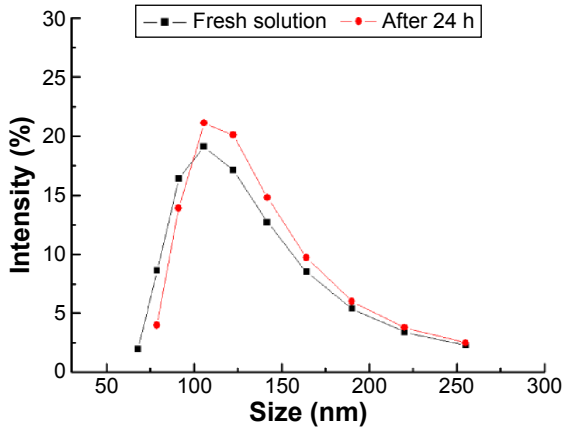

Figure S3 DLS diameters of pure MoS_2 nanosheets in saline before and after 24 hours.
Abbreviations: DLS, dynamic light scattering; h, hours.

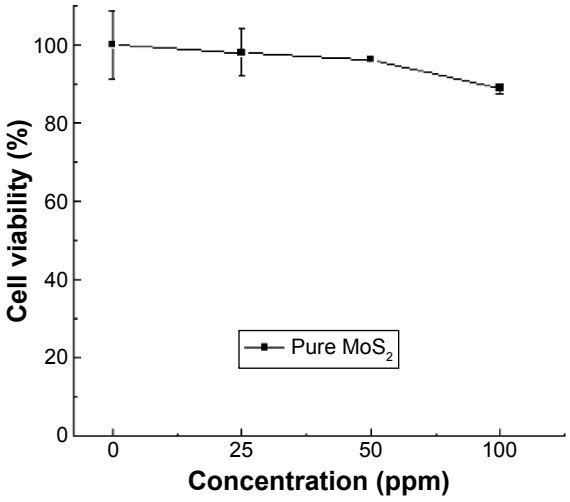

Figure S4 Cell viability assay of L929 cells after treatment with pure MoS_2 nanosheets at given Mo concentrations for 24 hours (mean ± SD, n=3).
Abbreviation: SD, standard deviation.

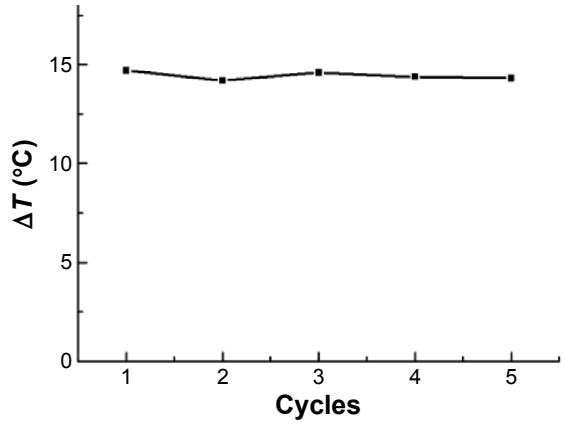

Figure S5 Temperature variations of SP-MoS_2 dispersion ([Mo] =100 ppm) under five cycles of continuous NIR irradiation (1.0 W/cm^2).
Abbreviations: SP-MoS_2, soybean phospholipid-encapsulated MoS_2; NIR, near-infrared; T, temperature.

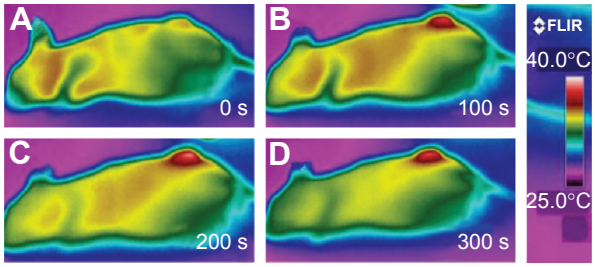

Figure S6 In vivo thermal images of mice injected with saline IV.
Notes: (**A**–**D**) Mouse was irradiated with NIR for 5 minutes, and the images were captured at different time points.
Abbreviations: IV, intravenous; NIR, near-infrared; s, seconds.

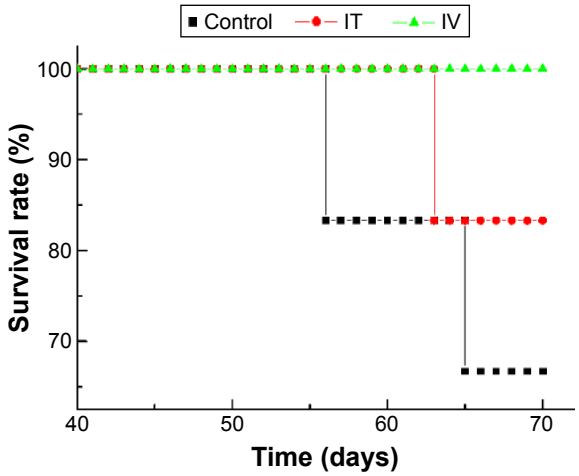

Figure S7 The survival rates of mice after different treatments.
Abbreviations: IV, intravenous; IT, intratumoral.

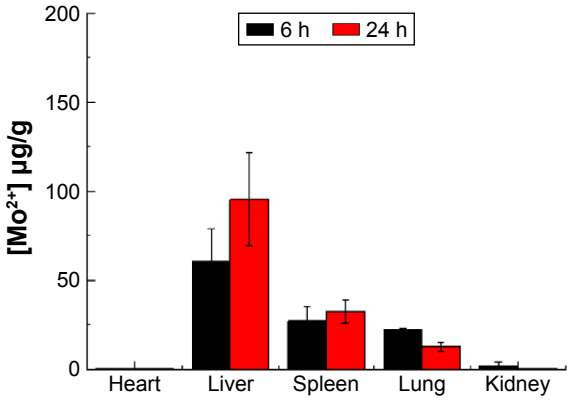

Figure S8 Biodistribution of Mo in major organs at different time points post IV injection (mean ± SD, n=3).
Abbreviations: IV, intravenous; SD, standard deviation; h, hours.